Plasmonic Activation of Dark Molecular Transitions Observable in the Far-Field

Mhamad Hantro[1], Bjorn Maes[2], Gilles Rosolen[2], Colin Van Dyck[1*]*

[1]Quantum Modeling of Nanosystems Group, Research Institute for Materials Science and Engineering, University of Mons, 20 Place du Parc, 7000 Mons, Belgium.

[2]Micro- and Nanophotonic Materials Group, Research Institute for Materials Science and Engineering, University of Mons, 20 Place du Parc, 7000 Mons, Belgium.

* mhamad.hantro@umons.ac.be

* colin.vandyck@umons.ac.be

ORCID

Mhamad Hantro: 0009-0000-3889-9750

Bjorn Maes: 0000-0003-3935-7990

Gilles Rosolen: 0000-0002-7399-3838

Colin Van Dyck: 0000-0003-2853-3821

Abstract:

The point-dipole approximation is commonly applied to simplify light-matter interactions. As previously reported, it is inaccurate near nanoplasmonic structures as those may strongly enhance higher-order multipoles. However, the enhancement of higher-order effects in the far-field, especially for dipole-forbidden molecular emitters, remains largely underexplored. In this study, we examine the breakdown of the point-dipole approximation for light emitted by four molecular systems, with dipole-allowed and dipole-forbidden transitions, all near an STM tip-like plasmonic structure. Importantly, we demonstrate that effects beyond dipolar and quadrupolar

orders are observable in both total decay and radiative rates, rendering typically dark molecular systems efficiently fluorescent in the far field. Radiative rates from the nanoplasmonic cavity exceed those of typical dipole-allowed molecular emitters and are thus predicted as observable in practical experiments.

Keywords: plasmonics, TD-DFT, Purcell enhancement, dipole-forbidden transitions, far-field, quantum emitters, quadrupole.

I. Introduction

Spontaneous emission is the process by which an excited molecule or atom returns to its ground state by emitting a photon. This process is commonly described using Fermi's Golden Rule, which links the decay rate to the interaction between the quantum emitter (QE) and the local density of photonic states (**LDOS**). In its simplest form, this interaction is modeled by using the point-dipole approximation (also known as the long-wavelength approximation[1]). It assumes that the molecule can be simplified as a point characterized by a transition dipole moment[2,3]. Under this assumption, two types of emitters can thus be distinguished, **dipole-allowed**, where the transition dipole moment is non-zero and emission occurs readily, and **dipole-forbidden**, where the transition dipole moment is effectively zero, resulting in extremely weak or suppressed emission (~ 3-4 orders of magnitude weaker)[4,5]. While dipole-allowed transitions dominate most optical properties of the molecule, the higher-order multipoles[6,4] can still reveal rich but often hidden details of the underlying molecular structure[7]. The latter is relevant in many fields such as organic light-emitting diodes[8,9], excitonic control[10,11], triplet exciton harvesting[12,13], and enhancing overall molecular sensing[14,15].

While the characteristics of the quantum emitter, as described above, are crucial in describing spontaneous emission, the other critical factor influencing the decay rate is the LDOS. Recent advancements in various nanoscale structures, such as nanospheres[16,17], nanoprisms[18,19], and 2D materials[4,20], all of which supports localized surface plasmon resonances, have emerged as powerful tools for strongly enhancing the

LDOS locally. It is well understood that the confinement results in significant amplification of the decay rates, even for weak or forbidden dipole transitions[4,21–24]. However, the emitted light is often strongly absorbed by the nanoplasmonic structure, eventually quenching emission in the far-field[25–29], *i.e.* quenching the radiative rate. Achieving a balance between confinement and radiative emission is critical and highly dependent on the nanoplasmonic architecture. This major concern triggered the interest in structures with high radiative efficiency (defined as the percentage of emitted photons that are not absorbed). This structural design often relies on the point-dipole approximation, which overlooks the complexities of the full molecular structure. Most notable structures are Metal-Insulator-Metal (MIM) structures[26,30] such as nanoparticles on mirrors[21], in addition to photonic crystals[31], and dielectric antennas[32].

Recently, optical imaging of molecules using scanning tunneling microscopy (STM)-tips has provided the ability to closely probe and manipulate molecule emitters: the emission of the molecule is observable in the far-field giving access to the Purcell enhancement (linewidth broadening). This technique was used in the context of electroluminescence[33,34], photoluminescence[35,36], manipulation of spin states[37,38], in addition to vibronic and Raman[39–41] spectroscopies. When these studies report the enhancement of the total and radiative decay rates of dipole-allowed emitters, it remains an open question whether it is possible to observe the enhancement of dipole-forbidden emitters, especially the radiative contribution. Previous works[6,42,43] have addressed the breakdown of the point-dipole approximation and the role of higher-order multipoles near nanoplasmonic structures, but the radiative contribution in the far-field for dipole-forbidden emitters remains less explored.

In this study, we investigate how plasmonic nanoscale structures influence the observation of light-emission in the far-field and reveal the important role played by higher-order effects. In particular, we compare point-dipole and point-quadrupole approximations with full molecular calculations and show that contributions beyond the quadrupolar order can shape both total decay and radiative rates in the STM-tip nanocavity. We focus on studying emission from the first excited S1 state of four molecular systems under a silver STM-tip, as represented in **Fig. 1 and 2**, which are chosen for their diverse optical properties. The α-quinquethiophene (5T) acts as a long-

conjugated emitter with a dipole-allowed transition. Octadecapentaene (ODP) is dipole-forbidden and characterized by a linear quadrupole moment. We also characterize two different α-quinquethiophene dimers configurations (5T-dimer). Due to excitonic coupling, the transition becomes dipole-forbidden and notably features a non-diagonal quadrupole. We observe substantial near- and far-field enhancements for dipole-forbidden emitters, with a prominent role played by higher-order effects. Interestingly, we indicate that the tip-substrate environment radiates 5 to 8% of the emitted photons. Benefiting from the very large Purcell enhancements, we show that this efficiency is high enough for these dipole-forbidden transitions to be observed in the far-field.

The manuscript is structured as follows. In Section II, we describe the methods and parameters used to compute the intrinsic and extrinsic optical properties of the emitters. Section III discusses the results and is divided into three subsections: the first focuses on the optical properties of the molecular emitters, the second reports the total decay rate enhancement, and the third presents the radiative contribution in the far-field. Finally, Section IV concludes with a summary of the key findings presented in this manuscript.

II. Methods

The electronic structure of each molecular system has been calculated with the TD-DFT method as implemented in Gaussian16[44], using the CAM-B3LYP[45] functional. All excited-state geometries were optimized using the 6-31+G(d,p) basis set. For the two 5T dimers, a single-point TD-DFT calculation was conducted by dimerizing the optimized structure of 5T, separating the monomers vertically by 3.8 Å, a value that is typical for $\pi - \pi$ stacked dimer structures[46], and further shifting one monomer with respect to the other by 0.5 Å along their long axis for the shifted dimer (see **Fig. 2**). This constitutes a model dimer system, representative of common structures that can be found in the literature, which usually are slightly shifted in plane[47]. It is important to note that the $2A_g$ state of ODP, characteristic of the polyene family, has been widely discussed in literature due to its double-excitation contribution[48,49], which is hard to capture using TD-DFT. For this reason, the emission wavelength of ODP was obtained based on experimental data[49]. The molecular structures are positioned under an STM tip made of silver, modeled as a

nanorod with a protrusion at its end (see **Fig. 1).** The tip is 1.5 nm above a dielectric spacer covering the silver substrate. A fully annotated schematic including all relevant distances is provided in **Figure 1**. . This choice is motivated by recent studies reporting the enhancement of light emission for single molecules probed by STM tips at the experimental level[50,51]. It has been shown that the tip with a protrusion model provided a reasonable agreement with experiments, explaining the efficient light confinement and enhancement of higher-order effects[6,52]. In line with those previous studies, we do not consider the excitation mechanism and assumed the emitters have been populated in their dark first excited states. Interestingly, the tunnelling excitation mechanism does not depend on the ground to first excited state dipole moment and shall apply equivalently to both dipole-allowed or dipole-forbidden emitters. The refractive index of the spacer is taken as n=1.5, while the permittivity of silver is described using the Johnson and Christy optical constants[53]. The tip radius is 3 nm. The length is systematically tuned from $L =$ 18.8 to 29.25 nm to ensure that the dipolar plasmonic mode is on resonance with the emission wavelength of the probed molecule (see Supplementary Material, Section 5). The molecules are placed 0.5 nm above the spacer (for the two dimers, it is the distance between the substrate and the lower molecule) in a 1.5 nm tip-spacer gap. The tip-spacer gap was kept constant to minimize variability in the plasmonic system.

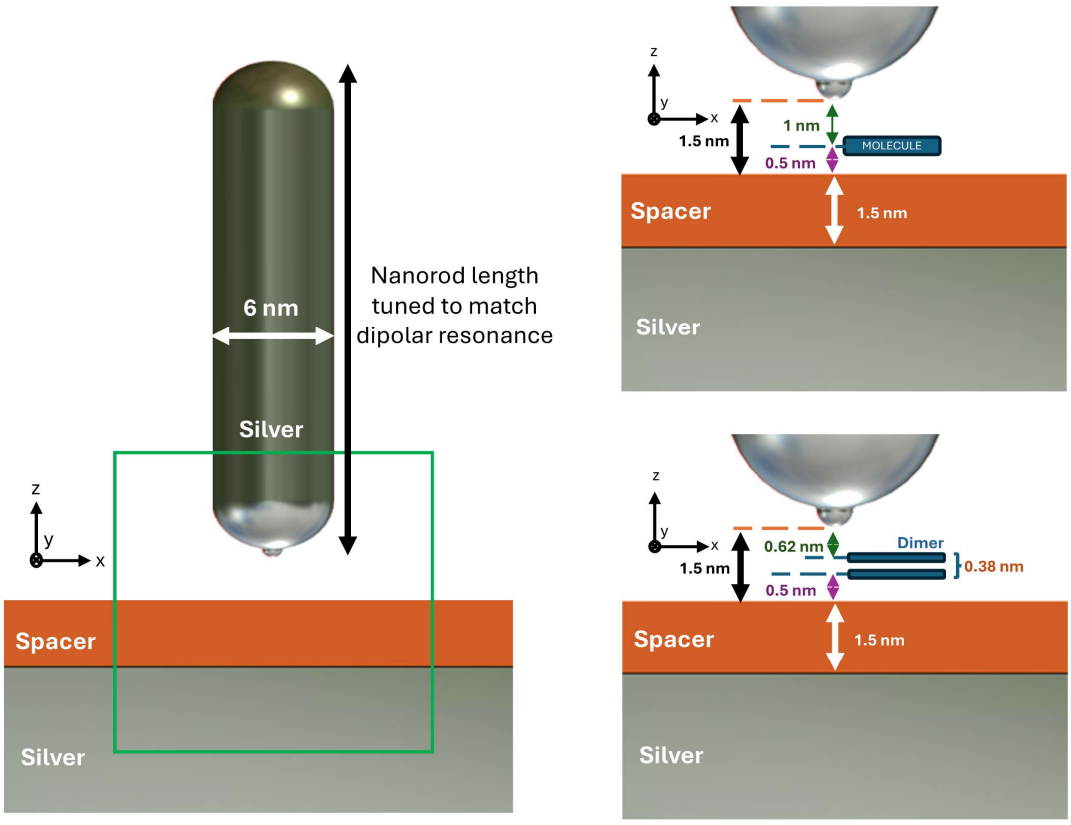

Figure 1 Molecular placement in STM tip-substrate nanoscale gap. *A schematic of the plasmonic structure, including dimensions (protrusion radius is 0.5 nm, see Supplementary Material, Section 5, for tip lengths), with all molecules assumed to be physisorbed at 0.5 nm above the dielectric spacer.*

In the following discussions, the molecules are assumed to lie parallel to the substrate (in the XY-plane, see **Fig. 1**), with their long axis oriented along the X-axis. According to Fermi's Golden Rule, the total rate can be calculated following[6]:

$$\Gamma = \frac{2\pi}{\hbar^2}\frac{e^2\hbar}{\pi\epsilon_0 c^2}\int\int \mathrm{d}^3\,\mathbf{r}\,\mathrm{d}^3\mathbf{r}'\,J_i(\mathbf{r})\left(\mathrm{Im}\,G_{ij}(\mathbf{r},\mathbf{r}',\omega_0)\right)J_j^*(\mathbf{r}') \qquad (1)$$

where $\hbar$ is the reduced Planck's constant, ϵ_0 is the dielectric permittivity of vacuum, ω_0 is the emission frequency, c is the speed of light, e is the elementary charge, $\mathbf{r}$ and $\mathbf{r}'$ are the spatial coordinates of an arbitrary electron in the system, G_{ij} is the i,j-component of the Green tensor, and J_i is the i^{th} component of the transition current density.

The rate Γ is calculated here by discretizing the current density of the emitter into a set of dipoles leading to (see Supplementary Material, Section 1)

$$\Gamma = \frac{2}{\hbar} \mathrm{Im}\left[\sum_k \boldsymbol{\mu}^{(k)} \cdot \mathbf{E}(\mathbf{r}_k)\right] \quad (2)$$

where $\boldsymbol{\mu}^{(k)}$ is the kth local dipole moment, and $\mathbf{E}(\mathbf{r}_k)$ is the electric field at its position. **Eq. 2** shows that the dipole discretization enables modeling the extended source within classical electromagnetic simulation software (here COMSOL) to calculate the rate. We follow this approach and the rate is calculated through the integration of the time-averaged Poynting vector, **S**, over a closed virtual surface enveloping all discretized dipole moments[54]. The radiative rate is calculated similarly with the integration taking place over the far-field boundaries. Details regarding our code implementation, referred as MIRAGE in the following, are explained in the Supplementary Material, Section 1.

Usually, the light-matter interaction is approximated by the multipolar expansion of the minimal-coupling interaction Hamiltonian[55,56]:

$$H_{int} = -\boldsymbol{\mu} \cdot \mathbf{E}(\mathbf{r}) - \mathbf{m} \cdot \mathbf{B}(\mathbf{r}) - \mathbf{Q} : \boldsymbol{\nabla}\mathbf{E}(\mathbf{r}) + \cdots, \quad (3)$$

where the emitter is represented in the first orders by a point at position $\mathbf{r}$ with an electric dipole $\boldsymbol{\mu}$, a magnetic dipole $\mathbf{m}$, and an electric quadrupole $\mathbf{Q}$. $\mathbf{E}$ ($\mathbf{B}$) is the electric (magnetic) field at the position $\mathbf{r}$ of the emitter. The emission rate is then proportional to the square of this Hamiltonian element computed between the ground and excited states, according to Fermi golden rule. This multipolar expansion provides an iterative model to understand the interplay between the dominant emitter transition moment and the electromagnetic modes of the structure. It also simplifies the analysis as the orders beyond the dipole term usually are negligible. Indeed, the size of molecular emitters is typically small compared to the emission wavelength and, for this reason, all these generally neglected terms are at the origin of 'higher order effects' in the literature[23,24,57,58]. Close to a nanoplasmonic structure, the effective wavelength and the size of the molecular emitter become comparable and we showed that this multipolar expansion turns out to be inadequate: it would require many terms going beyond the quadrupolar term[6]. The MIRAGE approach is an alternative that achieves high accuracy, similar to other methods[6], and accounts comprehensively for the entire set of higher-order multipole terms and their interferences without relying on a modal expansion of the Green tensor. The rate calculated with MIRAGE will thus be referred to as 'full' molecular

rate. It can be further compared with the multipolar expansion, considering only the interaction at the dipole or quadrupole order (which is the lowest non-vanishing moment for the dipole-forbidden molecules considered below). These approximations are referred to as the point-dipole approximation (PDA) or point-quadrupole approximation (PQA) in the following.

To ensure the reliability of our results, we performed comprehensive convergence tests. First, we verified the convergence of the meshes used to construct the transition current density (see Supplementary Material, Section 2.1). Second, we assessed the convergence of the COMSOL mesh refinement, in addition to the size of the inner domain (see Supplementary Material, Section 2.2). Noteworthy, our method to calculate the radiative rate neglects the quenching that may occur due to direct energy transfer between the excited molecule and the metal, without emission of a photon. However, Aguilar-Galindo et al.[28] showed that introducing a dielectric spacer strongly suppresses resonant electron transfer and it becomes negligible for NaCl spacers of about two monolayers and thicker. In our simulations, the molecule is located at 2 nm distance from the metal substrate, see Figure 1. The tip is kept at a distance from the molecule of 1 nm for the monomer and 0.62 nm for the dimer , thereby reducing electronic coupling. The remaining reduction of radiative emission is therefore electromagnetic in nature and is captured by the ohmic losses in the metal in the classical electrodynamics simulations.

III. Results and Discussions

In the following discussion, we start by characterizing the molecular emitters. Next, we calculate the total decay rates and finally, we assess the radiative decay rates.

1. Molecular emitters characterization

Fig. 2B reports the four studied molecular structures together with isosurfaces of the transition density corresponding to the first excited to ground state transition. The 5T density reveals that pairs of opposite charges are all contributing to the same direction which leads to a significant dipole for 5T, rationalizing the dipole-allowed character of the transition.

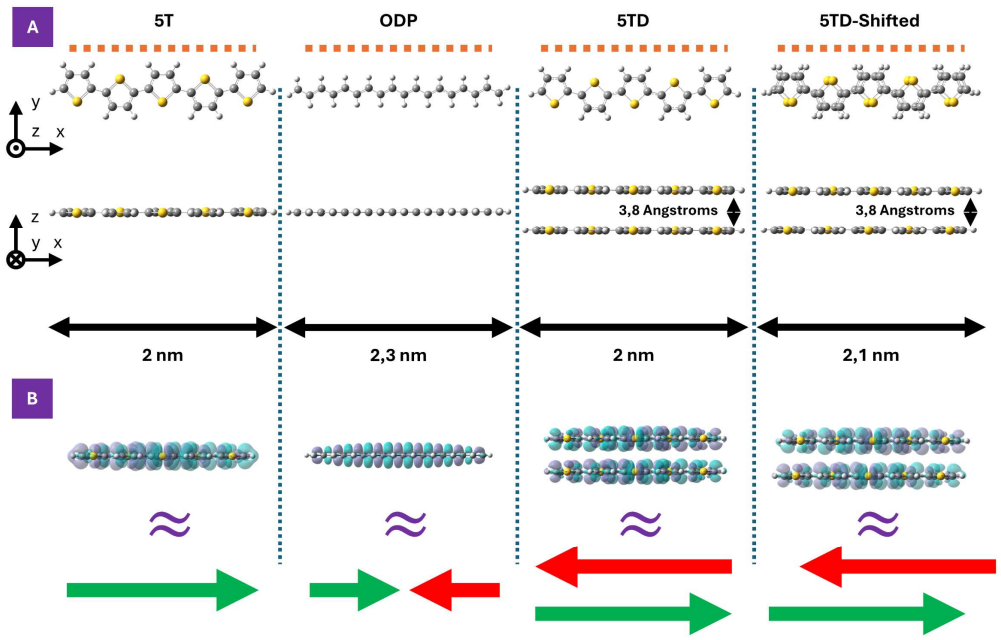

Figure 2 Molecular emitters. A) *The four molecules of interest displayed from top and side views, showing their lengths along the main axis.* ***B)*** *A visualization of their transition densities (side view only), and their visual analysis correspondence, where opposite colors indicate opposite transition charges, creating transition dipoles. This results in a dominant dipole for 5T (dipole-allowed), a linear quadrupole for ODP (dipole-forbidden), and two vertically shifted dipoles for the two 5T dimers, resulting mainly in a non-diagonal quadrupole.*

Conversely, the ODP shows a pattern of a central charge, with opposite charges on the edges, leading to two opposed canceling dipoles, rationalizing the dipole-forbidden character of the transition. Therefore, the transition is pictured by a linear quadrupole oriented along the conjugated backbone. Lastly, the two transition dipoles in the 5T dimers couple with opposite directions in the first excited state, leading to a dipole-forbidden transition (typically seen in H-aggregates[59]). Relative to their orientation, the transversal shift leads to a non-diagonal quadrupole, while the longitudinal shift gives rise to an additional linear quadrupole moment parallel to the long molecular axis. In **Table 1**, we present a summary of the main optical properties of the molecular systems.

Property	5T	ODP	5T-Dimer	Shifted 5T-Dimer
Emission Wavelength	510 nm	565 nm (exp)	654 nm	630 nm
Type of Transition	**Allowed**	**Forbidden**	**Forbidden**	**Forbidden**
Primary Transition Moment (in a.u.)	$\mu_x = 5.1$	$Q_{xx} = 9.36$	$Q_{xz} = 19.9$	$Q_{xx} = 4.8$ $Q_{xz} = 19.9$
Secondary Transition Moment(s) (in a.u.)	$O_{xxx} = 1960$	$H_{xxxx} = 3513$	$H_{xxxz} = 4120$	$H_{xxxx} = 2080$ $H_{xxxz} = 4120$

Table 1: *Main optical properties of the molecular systems under consideration, including emission wavelengths, type of transition, and primary and secondary transition moments.* ***μ****,* **Q**, **O**, *and* **H** *stand for* ***dipole***, ***quadrupole***, ***octupole*** *and* ***hexadecapole****, respectively.* *A.u. stands for atomic units.*

Having established the key optical properties of the molecular emitters, we now explore the total decay rates enhanced by their interaction with the near-field environment of the STM-tip. This system, with its sharp protrusion, serves as an excellent platform for studying light-matter interactions due to the intense electromagnetic hotspots and strong field gradients it generates. These gradients, shaped by the symmetry of the tip nodal planes, allow for enhanced coupling to higher-order multipoles, making it an ideal setup for activating forbidden transitions.

2. Total rates

We start by computing the total rates of the molecules under the tip as a function of their lateral displacement under the tip, along their main axis (assumed as the x-axis) from one exposed edge to the other. The total decay rates are reported in **Fig. 3** using the full molecular treatment and dipolar or quadrupolar approximation. The translation coordinate is defined as 0 when the emitter center of charge is directly beneath the tip and as -1/2 when the emitter is shifted half of its length to the left (its right edge is thus beneath the tip). The decay rate, $\gamma_{1ea_0}^{vac}$, is normalized to the decay rate of a one atomic unit dipole emitter in vacuum at the emitter wavelength. It is about 10^7 photons per second, a typical value for fluorescent molecular emitters. This normalization choice helps to appreciate the strong magnitude of light emission achieved in the systems,

where dipole-forbidden emitters become 10^3 times brighter than dipole-allowed emitters in vacuum for ODP (**Fig. 3B**) and 10^5 times for 5T (**Fig. 3C and D**).

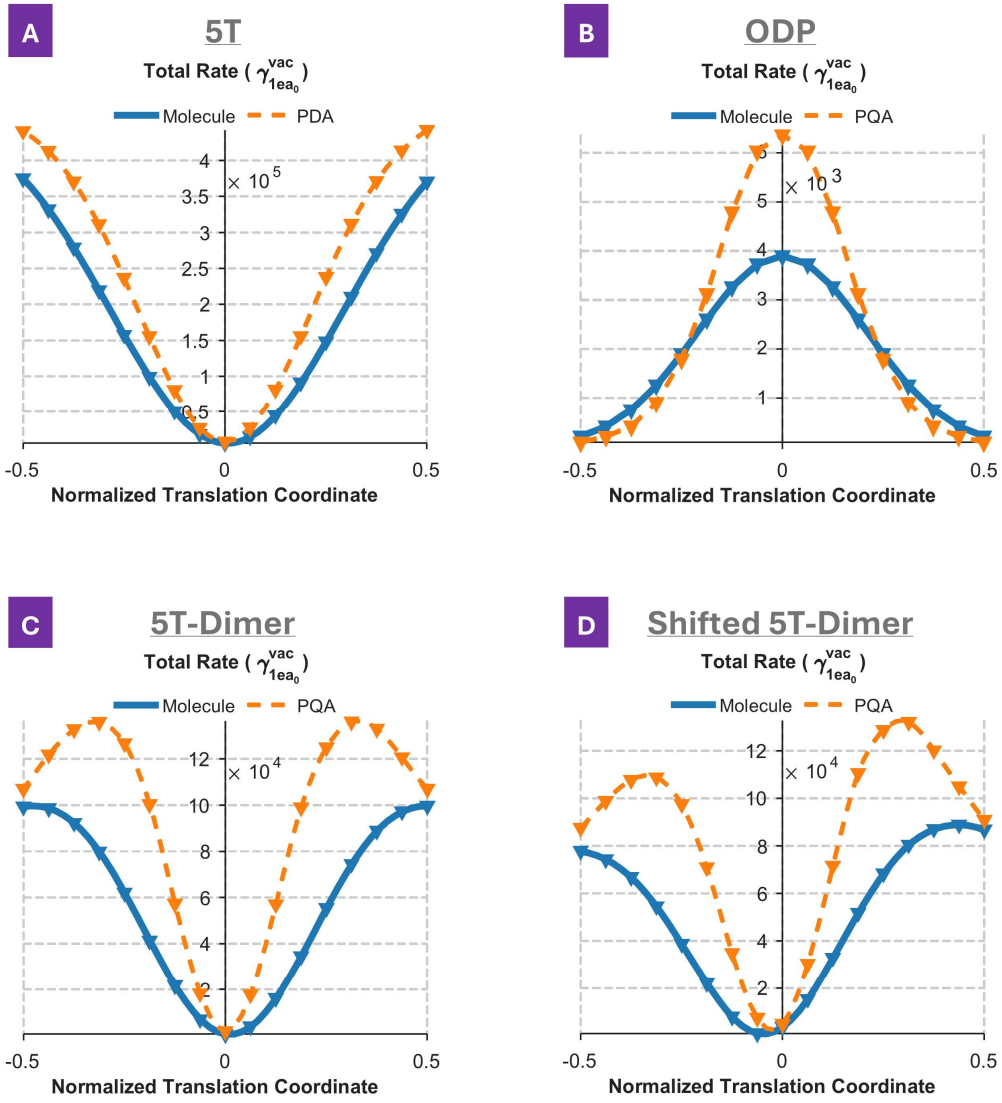

***Figure 3** **Dependence of the enhanced total decay rate with the translation of the four molecular emitters along their long axis.** The normalized translation coordinate corresponds to the translation of the molecule from one edge to the other under the tip. The origin corresponds to the molecule center of charge right under the tip.*

For the 5T molecule (**Fig. 3A**), a dipole-allowed emitter, we see a moderate deviation from the PDA as reported in previous studies[6,17,60]. This behavior is due to the delocalization of the exciton that can be observed in long conjugated emitters and the confinement of the field in the plasmonic environment. The rate is minimum when the center of the molecule is lying right under the tip, and maximum when the edges are

under the tip. This can be understood in light of the multipolar Hamiltonian **Eq. 3**, as given that the 5T molecule is primarily an x-oriented dipole moment, the interaction term $\boldsymbol{\mu} \cdot \mathbf{E}$ is therefore dominated by the x-component of the electric field (E_x). **Fig. 4A** displays this E_x component of the dipolar plasmonic mode, while **Fig. 4C** explicitly plots E_x (blue dashed line) along the translation axis. This plot reveals a field node at the center (x=0), and field maxima lying beside the tip, explaining the trend of the rate observed in **Fig. 3A**.

In contrast, the ODP molecule (**Fig. 3B**) shows a behavior opposite to the dipole enhancement pattern. The decay rate peaks at the center and decreases as the edges of the molecule get exposed to the tip. This behavior arises from the antisymmetric nature of the x-component plasmonic dipole mode around the central node (see **Fig. 4A**), generating a strong gradient that couples efficiently with the large Q_{xx} linear quadrupole of ODP. Indeed, unlike a dipole transition which is enhanced by the magnitude of the field, a quadrupolar transition is enhanced by the gradient of the field (see **Eq. 3**). Surprisingly, the emission rate of a point-quadrupole using the computed molecular moment shows deviations from the full molecule rate. At the center, the point-quadrupole approximation predicts a significantly larger enhancement, resulting in an overestimation of about 63%. This overestimation decreases rapidly as the molecule edge gets exposed to the tip, eventually turning into an underestimation of about 60%. The crossing is due to the pinpoint nature of the point-quadrupole: the rate follows closely the magnitude of the field gradient in contrast to the extended molecule that still has a significant part affected by the strong gradient. This significant relative error highlights that approximating the molecular emitter as a point-quadrupole moment is not sufficient, as higher-order moments beyond quadrupole induce substantial effects.

We now compare both 5T dipole-forbidden dimers (**Fig. 3C** and **D**) to the other two molecules. In fact, the dimers approximately share the same rate pattern as the dipole-allowed molecule as the rate shows a similar dip right at (5T-dimer) or near (shifted 5T-dimer) the center. Recalling that their transition is mainly characterized by a non-diagonal quadrupole contribution, we see that this type of quadrupole interacts completely differently from the ODP linear quadrupole within the same structure.

Interestingly, the peak-to-valley difference is larger by 12% for the shifted dimer. Also, we observe an additional asymmetry for this emitter (**Fig. 3D**). This suggests that the additional contribution of the linear quadrupole (see **Table 1**) interferes with the non-diagonal component, giving rise to constructive or destructive effects, as further detailed below. We also attribute the minor shift of the minimum position toward the left side to interference effects, since this behavior is also observable at the PQA level. Counterintuitively, while the upper molecule extends further to the right of the dimer (see **Fig. 2**), the decay rate is smaller by 9% when the right edge is exposed rather than the left edge (**Fig. 3D**). This observation challenges the simplistic expectation that a shorter tip-molecule distance would lead to a higher decay rate.

Noticing that the PQA follows the same asymmetry, we make use of the intuitive picture of the multipolar Hamiltonian (see **Eq. 3**) to explain its origin, keeping only the quadrupolar order:

$$H_{int} = Q_{xx}\partial_x E_x + Q_{xz}(\partial_x E_z + \partial_z E_x) \;=\; Q_{xx}\partial_x E_x + 2Q_{xz}(\partial_x E_z) \quad . \qquad (4)$$

We used the fact that $Q_{zx} = Q_{xz}$ and $\partial_x E_x = \partial_x E_z$ (see supplementary section 4). To quantify the emission rate, this Hamiltonian element is squared according to Fermi golden rule, leading to two positive direct terms and a signed crossed interference term. The two primary non-zero components, Q_{xx} and Q_{xz}, as shown in **Table 1** for the shifted 5T dimer, share the same sign and thus the sign of the interference term is driven by the relative signs of the two field-components derivatives. This implies that the highest decay rate is expected at positions where the two relevant field gradients exhibit the same sign. We show in **Fig. 4C** a graph of the field along the displacement line of the molecule (defined by the center of the dimer) on the x-axis, computed for the x- and z-components of the dipolar plasmon mode of the structure. We note that the modal simulation was performed without the dielectric layer as its inclusion greatly increases the computational cost for an impact that would be limited to a shift of the mode resonance frequency of the STM tip[61].

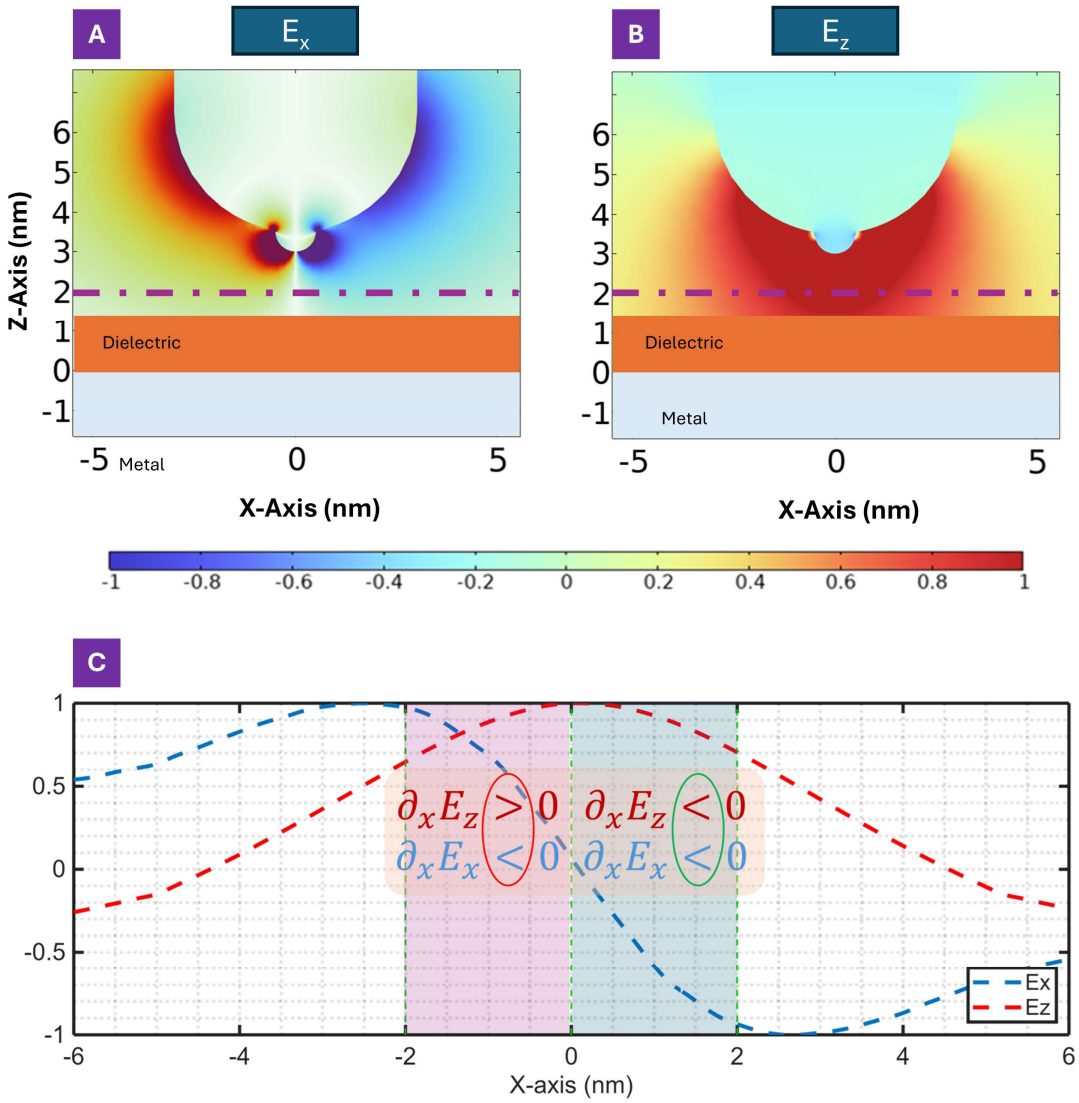

***Figure 4** Dipolar plasmonic mode plotted in the XZ plane for **(A)** the x-component and **(B)** z-component of the field. **(C) Visual normal mode analysis:** The x-(blue dashed curve), z-(red dashed curve) components, normalized to their maximum, of the dipolar plasmonic mode (in arbitrary units) are plotted along the dashed displacement line (highlighted in purple in A and B). The light blue (purple) shaded region corresponds to the area where the molecule is displaced to the right (left) side of the tip. The derivatives of the dipolar mode components along this axis, written on top, have the same sign on the right, and opposite signs on the left. We note that the dielectric layer in (A) is added for visualization purposes, however, it was not modeled in the eigenfrequency simulation.*

Looking at the blue light shaded region of **Fig. 4C**, equivalent to the right side of **Fig. 3D**, both derivatives of the field have the same sign, resulting in a constructive interference and an increased total decay rate. In the purple shaded region of **Fig. 4C**, equivalent to

the left side of **Fig. 3D**, however, the derivatives have opposite signs, resulting in a destructive interference and a reduction in the total decay rate. This simple illustration rationalizes the asymmetric behavior observed in **Fig. 3D**, including the displacement of the minimum toward the left side. Notably, while the PQA accurately captures the asymmetry, it consistently overestimates the decay rate throughout the translation. Moreover, it predicts a premature peak that is absent in the full molecular treatment, highlighting some of its limitations.

Up until now, we have focused mainly on the qualitative nature of the decay rates. On the quantitative side, however, we see that these dipole-forbidden molecules exhibit impressive decay rates, ranging from around $\mathbf{4 \times 10^3}$ for ODP to as high as $\mathbf{10^5}$ for the dimer. We stress that the latter absolute decay rate approaches the magnitude of the strongly enhanced dipole-allowed emitter (5T molecule). Overall, these rates suggest that the dark molecular structures can emit thousands of times more intensely than a dipole emitter in vacuum. However, this narrative misses on a very important issue that correlates with strong confinements: structural absorption.

3. Radiative rates

Plasmonic nanostructures sustain strongly confined fields that effectively enhance the decay rate of transitions beyond the dipole approximation. However, such plasmonic mode suffers from losses that reduce the radiative efficiency[26,30]. Nonetheless, the radiation into plasmons can still be harvested through suitable out-coupling techniques, such as the particle or tip on mirror setups[26], as we show in this section. In **Fig. 5**, we report the calculated radiative rates, and in **Fig. 6** the far-field efficiencies, for the molecular structures studied in the previous section. We used the same normalization convention as used in the previous section, with rates normalized versus a one-atomic-unit dipole emitter placed in vacuum.

Importantly, our calculations predict a strong enhancement observable in the far-field emission. Both 5T dimers (**Fig. 5C** and **D**), H-aggregate configurations with a non-diagonal quadrupole moment, achieve radiative rates that are comparable to the dipole-allowed 5T emitter (**Fig. 5A**) within the same plasmonic environment. In comparison to a dipole-allowed emitter in vacuum, the emission rate of the dimer is about 8000 times

brighter, despite its dipole-forbidden nature. We note that, because the dimers are extended along the z-axis, one might reasonably attribute their large radiative enhancement to a reduced tip–molecule separation. To address this possibility, we recomputed the rates for 5TD while maintaining a 1 nm fixed tip-molecule separation (see Supplementary Material, Section 6). Besides a reduction in rates of a factor of 10, the principal conclusions presented above remain.

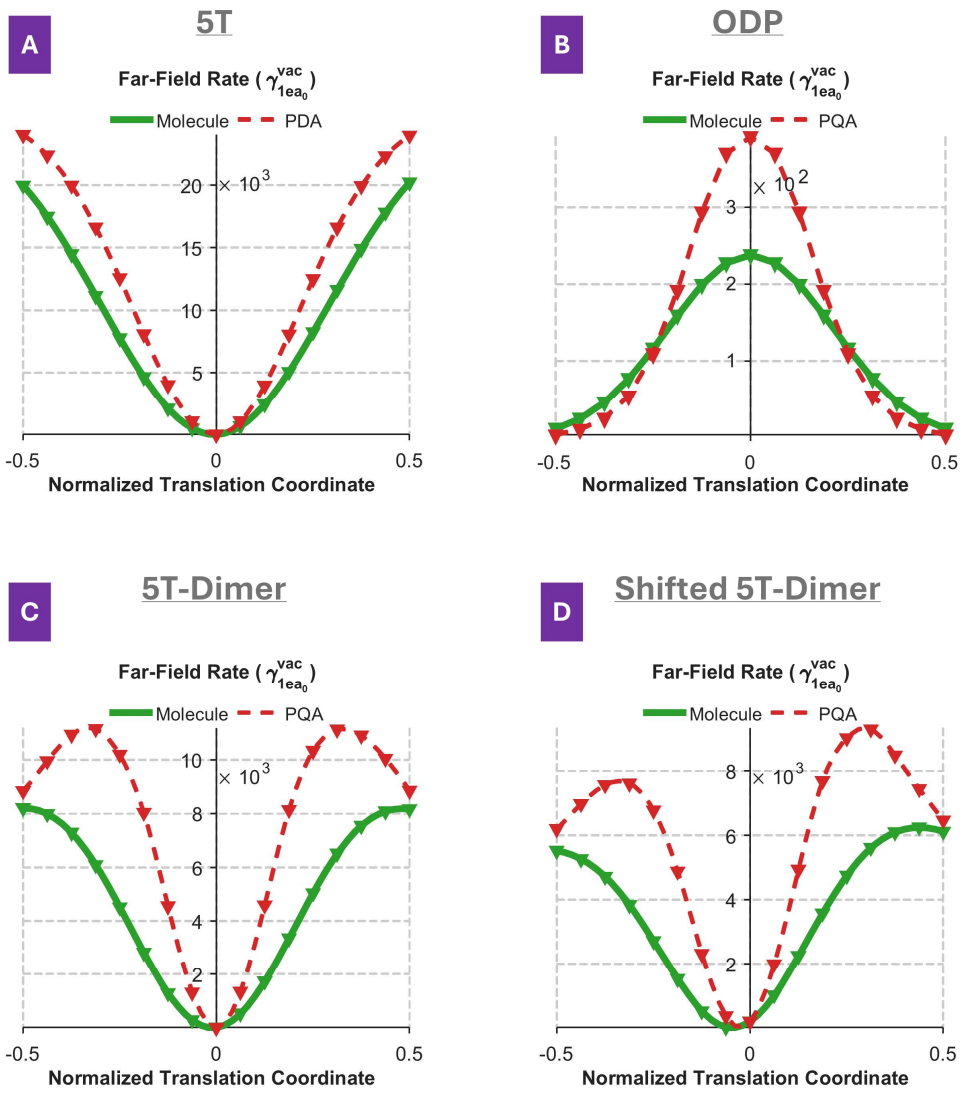

***Figure 5** The radiative rates of A) 5T, B) ODP, and C-D) the two 5T-dimers, comparing the PD(Q)A with full molecular structure calculations, plotted against the normalized translation coordinate.*

Additionally, the ODP molecule (**Fig. 5B**), behaving as a linear quadrupole, also exhibits significant radiative rates. These are however less intense than for the dimer, with an emission rate about 230 times the emission rate of a dipole-allowed emitter in vacuum. Furthermore, we see that the rate trend observed in the near-field (**Fig. 4**) is reflected in the radiative rates. This similarity indicates that the characterization done in the near-field, including deviations due to higher-order terms, leads to equivalent conclusions in the far-field.

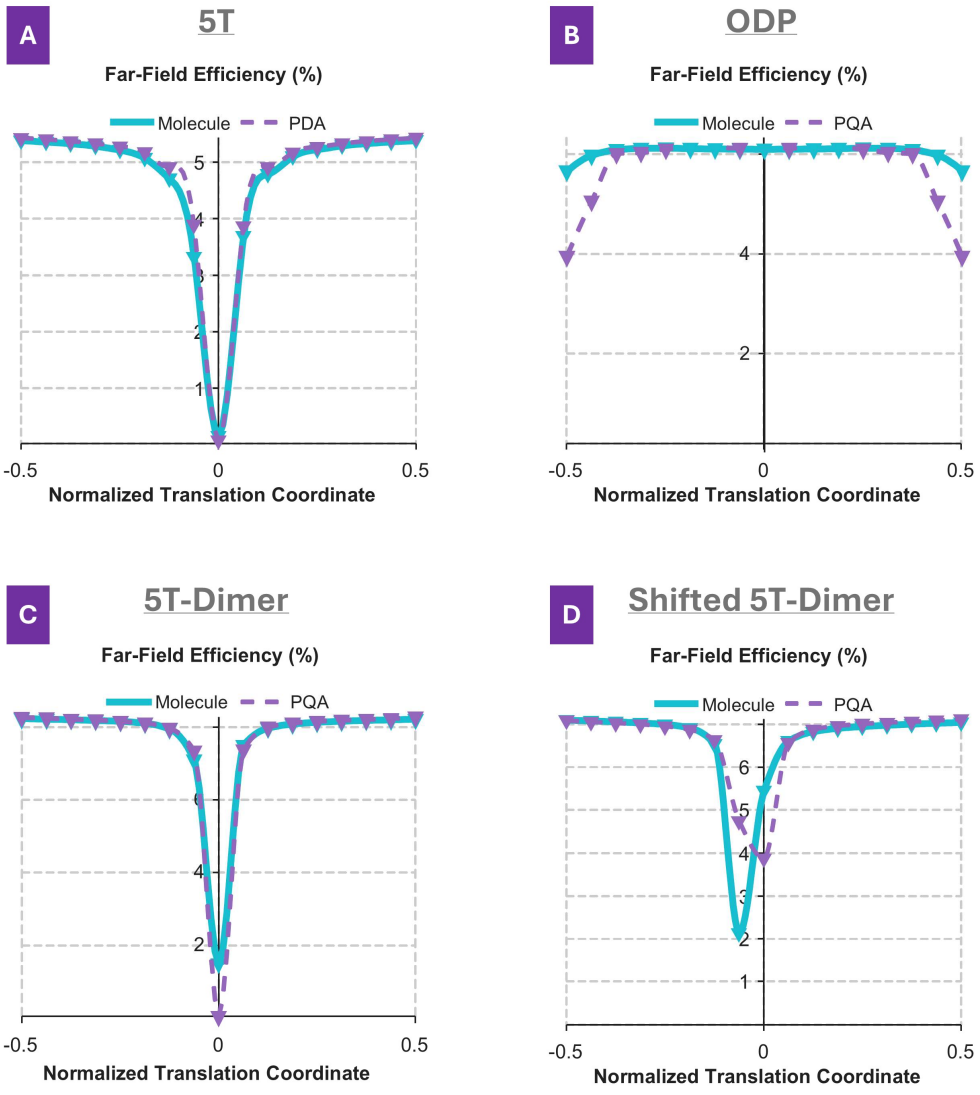

***Figure 6** The far-field efficiencies of A) 5T, B) ODP, and C-D) the two 5T-dimers, comparing the PD(Q)A with full molecular structure calculations, plotted against the normalized translation coordinate.*

Radiative efficiencies are reported in **Fig. 6**. We observe that these are rather similar (between 5-8%) and that efficiencies of the total decay rate closely follow the far-field efficiencies of the respective point approximations. Interestingly, the efficiencies are slightly higher for the dipole-forbidden emitters. Also, we note differences for both dimers (**Fig. 6C and D**) at the center. For the first (**Fig. 6C**), as the radiative rate approaches 0, small fluctuations in the radiative rates become non-negligible. For the second (**Fig. 6D**), the positional shift of the minimum is attributed to interferences. The similarity in the radiative efficiencies profiles is attributed to the radiative efficiency of the dipolar mode of the tip, as all these emitters are mainly coupled to this mode. Finally, variations in the maximum efficiencies arise from differences in tip lengths (adjusted to tune the dipolar resonance) and from the dispersion of silver, which affects the intrinsic radiative efficiency of the dipolar modes. This suggests that the PD(Q)A level theory is sufficient for the most part in characterizing the far-field efficiency of a given plasmonic system with high accuracy. The results also reveal that emission beyond dipolar transition is not inevitably quenched and thus exploitable. Noteworthy, high efficiencies about 50% have already been mentioned in literature for similar metal on mirror structures, at the point-dipole level of approximation[62]. This suggests that inclusion of a high refractive index material around the emitters may further improve those radiative efficiencies.

IV. Conclusion

In this work, we calculated the decay rate of both dipole-allowed and dipole-forbidden emitters under an STM-tip configuration and compared the total decay rate obtained from a full molecular description with predictions from the point-dipole and point-quadrupole approximations. First, we show that the usual point approximations, both PDA and PQA, are insufficient to accurately predict the total decay rates of the considered emitters. For the dipole-allowed molecule (5T), the point-dipole approximation showed its typical limitation by providing a qualitatively reasonable description, while failing quantitatively (~15% error). However, for the dipole-forbidden emitters (ODP and the two 5T-dimers), the PQA can overestimate or underestimate the total rate by close to 100%, missing critical interference and higher-order multipolar effects. This also leads to qualitative differences in the shape of the emission profile.

Second, we demonstrate that dipole-forbidden transitions can become bright in plasmonic environments. Notably, dipole-forbidden emitters like ODP and the 5T-dimers exhibit total decay rates ranging from factors around 4×10^3 to 10^5 times higher than a dipole in vacuum. Importantly, their radiative rates in the far-field are up to 8000 times larger, making them experimentally observable. This is attributed to the dipolar mode coupling with the STM-tip on mirror environment that demonstrates a radiative efficiency up to 8%. These numbers provide a favorable answer to the common question whether non-dipolar transitions would be observable because of inevitable quenching by the metals. Hence, dipole-forbidden molecules can be activated with strong radiative rates far surpassing dipole-allowed molecules in vacuum. This theoretically demonstrates the possibility to switch dark molecular transitions into bright and observable ones.

Higher-order effects are intrinsically rich and open new strategies to control and design light emission at the nanoscale, by exploiting moments and interference effects beyond the dipolar term. We show that the choice of the molecular structure can drastically change emission characteristics. Those can then easily be tuned from chemical design. Finally, higher-order effects can be used to exploit and reveal usually dark features in nanodevices.

Acknowledgments

We acknowledge the support from Actions de Recherche Concertées (project ARC-21/25 UMONS2), FRS-FNRS (PDR project T.0166.20). We acknowledge CECI (Consortium des Équipements de Calcul Intensif) for access to their computational equipment.

Author contributions

M. Hantro conducted the research and performed simulations. B. Maes, G. Rosolen and C. Van Dyck supervised the research. All authors contributed to the manuscript writing.

Conflict of interest

Authors state no conflict of interest.

Data availability statement

The datasets generated and/or analyzed during the current study are available from the corresponding author upon reasonable request.

References

(1) Cohen-Tannoudji, C.; Dupont-Roc, J.; Grynberg, G. Photons and Atoms-Introduction to Quantum. *Photons and Atoms-Introduction to Quantum Electrodynamics* **1997**, 486.

(2) Novotny, L.; Hecht, B. *Principles of Nano-Optics*, 2nd ed.; Cambridge University Press: Cambridge, 2012. https://doi.org/10.1017/CBO9780511794193.

(3) Sakurai, J. J.; Napolitano, J. *Modern Quantum Mechanics*, Third edition.; Cambridge University Press: Cambridge, 2020.

(4) Rosolen, G.; Maes, B. Strong Multipolar Transition Enhancement with Graphene Nanoislands. *APL Photonics* **2021**, *6* (8), 1–9. https://doi.org/10.1063/5.0053234.

(5) Rivera, N.; Kaminer, I.; Zhen, B.; Joannopoulos, J. D.; Soljačić, M. Shrinking Light to Allow Forbidden Transitions on the Atomic Scale. *Science* **2016**, *353* (6296), 263–269. https://doi.org/10.1126/science.aaf6308.

(6) Hantro, M.; Maes, B.; Rosolen, G.; Van Dyck, C. Higher-Order Effects and Validity of the Point-Dipole Approximation for Conjugated Extended Molecular Emitters near Plasmonic Nanostructures. *The Journal of Chemical Physics* **2025**, *162* (3), 034303. https://doi.org/10.1063/5.0242123.

(7) Cuartero-González, A.; Fernández-Domínguez, A. I. Dipolar and Quadrupolar Excitons Coupled to a Nanoparticle-on-Mirror Cavity. *Phys. Rev. B* **2020**, *101* (3), 035403. https://doi.org/10.1103/PhysRevB.101.035403.

(8) Lee, H.; Nam, H.; Yeo, H.-J.; Yang, H.; Kim, T. High Efficiency over 15% by Breaking the Theoretical Efficiency Limit of Fluorescent Organic Light-Emitting Diodes with Localized Surface Plasmon Resonance Effects. *ACS Appl. Mater. Interfaces* **2023**, *15* (29), 35290–35301. https://doi.org/10.1021/acsami.3c07064.

(9) Chou, C.-H.; Chen, F.-C. Plasmonic Nanostructures for Light Trapping in Organic Photovoltaic Devices. *Nanoscale* **2014**, *6* (15), 8444–8458. https://doi.org/10.1039/C4NR02191F.

(10) Spano, F. C.; Silva, C. H- and J-Aggregate Behavior in Polymeric Semiconductors. *Annu. Rev. Phys. Chem.* **2014**, *65* (1), 477–500. https://doi.org/10.1146/annurev-physchem-040513-103639.

(11) Brédas, J.-L.; Norton, J. E.; Cornil, J.; Coropceanu, V. Molecular Understanding of Organic Solar Cells: The Challenges. *Acc. Chem. Res.* **2009**, *42* (11), 1691–1699. https://doi.org/10.1021/ar900099h.

(12) Bujak, Ł.; Narushima, K.; Sharma, D. K.; Hirata, S.; Vacha, M. Plasmon Enhancement of Triplet Exciton Diffusion Revealed by Nanoscale Imaging of Photochemical Fluorescence Upconversion. *J. Phys. Chem. C* **2017**, *121* (45), 25479–25486. https://doi.org/10.1021/acs.jpcc.7b08495.

(13) Polak, D.; Jayaprakash, R.; P. Lyons, T.; Á. Martínez-Martínez, L.; Leventis, A.; J. Fallon, K.; Coulthard, H.; G. Bossanyi, D.; Georgiou, K.; Anthony J. Petty, I. I.; Anthony, J.; Bronstein, H.; Yuen-Zhou, J.; I. Tartakovskii, A.; Clark, J.; J. Musser, A. Manipulating Molecules with Strong Coupling: Harvesting Triplet Excitons in Organic Exciton Microcavities. *Chemical Science* **2020**, *11* (2), 343–354. https://doi.org/10.1039/C9SC04950A.

(14) Yu, R.; Cox, J. D.; de Abajo, F. J. G. Nonlinear Plasmonic Sensing with Nanographene. *Phys. Rev. Lett.* **2016**, *117* (12), 123904. https://doi.org/10.1103/PhysRevLett.117.123904.

(15) Cortijo-Campos, S.; Ramírez-Jiménez, R.; de Andrés, A. Raman and Fluorescence Enhancement Approaches in Graphene-Based Platforms for Optical Sensing and Imaging. *Nanomaterials* **2021**, *11* (3), 644. https://doi.org/10.3390/nano11030644.
(16) Luo, D.; Shi, B.; Zhu, Q.; Qian, L.; Qin, Y.; Xie, J. Optical Properties of Au–Ag Nanosphere Dimer: Influence of Interparticle Spacing. *Optics Communications* **2020**, *458*, 124746. https://doi.org/10.1016/j.optcom.2019.124746.
(17) Zhang, Y.; Dong, Z. C.; Aizpurua, J. Influence of the Chemical Structure on Molecular Light Emission in Strongly Localized Plasmonic Fields. *Journal of Physical Chemistry C* **2020**, *124* (8), 4674–4683. https://doi.org/10.1021/acs.jpcc.9b10256.
(18) Takeshima, N.; Sugawa, K.; Tahara, H.; Jin, S.; Wakui, H.; Fukushima, M.; Tokuda, K.; Igari, S.; Kanakubo, K.; Hayakawa, Y.; Katoh, R.; Takase, K.; Otsuki, J. Plasmonic Silver Nanoprism-Induced Emissive Mode Control between Fluorescence and Phosphorescence of a Phosphorescent Palladium Porphyrin Derivative. *ACS Nano* **2019**, *13* (11), 13244–13256. https://doi.org/10.1021/acsnano.9b06269.
(19) Xu, X.; Yi, Z.; Li, X.; Wang, Y.; Liu, J.; Luo, J.; Luo, B.; Yi, Y.; Tang, Y. Tunable Nanoscale Confinement of Energy and Resonant Edge Effect in Triangular Gold Nanoprisms. *J. Phys. Chem. C* **2013**, *117* (34), 17748–17756. https://doi.org/10.1021/jp4051929.
(20) Poddubny, A. N.; Belov, P. A.; Ginzburg, P.; Zayats, A. V.; Kivshar, Y. S. Microscopic Model of Purcell Enhancement in Hyperbolic Metamaterials. *Phys. Rev. B* **2012**, *86* (3), 035148. https://doi.org/10.1103/PhysRevB.86.035148.
(21) Huang, J.; Ojambati, O. S.; Climent, C.; Cuartero-Gonzalez, A.; Elliott, E.; Feist, J.; Fernández-Domínguez, A. I.; Baumberg, J. J. Influence of Quadrupolar Molecular Transitions within Plasmonic Cavities. *ACS Nano* **2024**, *18* (22), 14487–14495. https://doi.org/10.1021/acsnano.4c01368.
(22) García-Puente, Y.; Kashyap, R. Magnetic Purcell Enhancement in a Nanoantenna-Spherical Bragg Resonator Coupled System. *Annalen der Physik* **2023**, *535* (11), 2300147. https://doi.org/10.1002/andp.202300147.
(23) Smeets, S.; Maes, B.; Rosolen, G. General Framework for Two-Photon Spontaneous Emission near Plasmonic Nanostructures. *Phys. Rev. A* **2023**, *107* (6), 063516. https://doi.org/10.1103/PhysRevA.107.063516.
(24) Smeets, S.; Maes, B.; Rosolen, G. Interference between Multipolar Two-Photon Transitions in Quantum Emitters near Plasmonic Nanostructures. *Discover Nano* **2024**, *19* (1), 155. https://doi.org/10.1186/s11671-024-04111-8.
(25) Kongsuwan, N.; Demetriadou, A.; Chikkaraddy, R.; Benz, F.; Turek, V. A.; Keyser, U. F.; Baumberg, J. J.; Hess, O. Suppressed Quenching and Strong-Coupling of Purcell-Enhanced Single-Molecule Emission in Plasmonic Nanocavities. *ACS Photonics* **2018**, *5* (1), 186–191. https://doi.org/10.1021/acsphotonics.7b00668.
(26) Yang, J.; Faggiani, R.; Lalanne, P. Light Emission in Nanogaps: Overcoming Quenching. *Nanoscale Horiz.* **2015**, *1* (1), 11–13. https://doi.org/10.1039/C5NH00059A.
(27) Su, Q.; Jiang, C.; Gou, D.; Long, Y. Surface Plasmon-Assisted Fluorescence Enhancing and Quenching: From Theory to Application. *ACS Appl. Bio Mater.* **2021**, *4* (6), 4684–4705. https://doi.org/10.1021/acsabm.1c00320.
(28) Aguilar-Galindo, F.; Zapata-Herrera, M.; Díaz-Tendero, S.; Aizpurua, J.; Borisov, A. G. Effect of a Dielectric Spacer on Electronic and Electromagnetic Interactions at Play in Molecular Exciton Decay at Surfaces and in Plasmonic Gaps. *ACS Photonics* **2021**, *8* (12), 3495–3505. https://doi.org/10.1021/acsphotonics.1c00791.
(29) Ko, C.-T.; Han, Y.-Y.; Chen, C.-H.; Shieh, J.; Chen, M.-J. Enormous Plasmonic Enhancement and Suppressed Quenching of Luminescence from Nanoscale ZnO Films by Uniformly Dispersed Atomic-Layer-Deposited Platinum with Optimized Spacer Thickness. *J. Phys. Chem. C* **2013**, *117* (49), 26204–26212. https://doi.org/10.1021/jp406156n.

(30) Faggiani, R.; Yang, J.; Lalanne, P. Quenching, Plasmonic, and Radiative Decays in Nanogap Emitting Devices. *ACS Photonics* **2015**, *2* (12), 1739–1744. https://doi.org/10.1021/acsphotonics.5b00424.
(31) Patterson, M.; Hughes, S.; Dalacu, D.; Williams, R. L. Broadband Purcell Factor Enhancements in Photonic-Crystal Ridge Waveguides. *Phys. Rev. B* **2009**, *80* (12), 125307. https://doi.org/10.1103/PhysRevB.80.125307.
(32) Regmi, R.; Berthelot, J.; Winkler, P. M.; Mivelle, M.; Proust, J.; Bedu, F.; Ozerov, I.; Begou, T.; Lumeau, J.; Rigneault, H.; García-Parajó, M. F.; Bidault, S.; Wenger, J.; Bonod, N. All-Dielectric Silicon Nanogap Antennas To Enhance the Fluorescence of Single Molecules. *Nano Lett.* **2016**, *16* (8), 5143–5151. https://doi.org/10.1021/acs.nanolett.6b02076.
(33) Luo, Y.; Kong, F.-F.; Tian, X.-J.; Yu, Y.-J.; Jing, S.-H.; Zhang, C.; Chen, G.; Zhang, Y.; Zhang, Y.; Li, X.-G.; Zhang, Z.-Y.; Dong, Z.-C. Anomalously Bright Single-Molecule Upconversion Electroluminescence. *Nat Commun* **2024**, *15* (1), 1677. https://doi.org/10.1038/s41467-024-45450-5.
(34) Rai, V.; Gerhard, L.; Balzer, N.; Valášek, M.; Holzer, C.; Yang, L.; Wegener, M.; Rockstuhl, C.; Mayor, M.; Wulfhekel, W. Activating Electroluminescence of Charged Naphthalene Diimide Complexes Directly Adsorbed on a Metal Substrate. *Phys. Rev. Lett.* **2023**, *130* (3), 036201. https://doi.org/10.1103/PhysRevLett.130.036201.
(35) Yang, B.; Chen, G.; Ghafoor, A.; Zhang, Y.-F.; Zhang, X.-B.; Li, H.; Dong, X.-R.; Wang, R.-P.; Zhang, Y.; Zhang, Y.; Dong, Z.-C. Chemical Enhancement and Quenching in Single-Molecule Tip-Enhanced Raman Spectroscopy. *Angewandte Chemie International Edition* **2023**, *62* (13), e202218799. https://doi.org/10.1002/anie.202218799.
(36) Doležal, J.; Canola, S.; Hapala, P.; de Campos Ferreira, R. C.; Merino, P.; Švec, M. Real Space Visualization of Entangled Excitonic States in Charged Molecular Assemblies. *ACS Nano* **2022**, *16* (1), 1082–1088. https://doi.org/10.1021/acsnano.1c08816.
(37) de Campos Ferreira, R. C.; Sagwal, A.; Doležal, J.; Canola, S.; Merino, P.; Neuman, T.; Švec, M. Resonant Tip-Enhanced Raman Spectroscopy of a Single-Molecule Kondo System. *ACS Nano* **2024**, *18* (20), 13164–13170. https://doi.org/10.1021/acsnano.4c02105.
(38) Yamamoto, S.; Imada, H.; Kim, Y. Atomic-Scale Photon Mapping Revealing Spin-Current Relaxation. *Phys. Rev. Lett.* **2022**, *128* (20), 206804. https://doi.org/10.1103/PhysRevLett.128.206804.
(39) Doppagne, B.; Chong, M. C.; Bulou, H.; Boeglin, A.; Scheurer, F.; Schull, G. Electrofluorochromism at the Single-Molecule Level. *Science* **2018**, *361* (6399), 251–255. https://doi.org/10.1126/science.aat1603.
(40) Kong, F.-F.; Tian, X.-J.; Zhang, Y.; Yu, Y.-J.; Jing, S.-H.; Zhang, Y.; Tian, G.-J.; Luo, Y.; Yang, J.-L.; Dong, Z.-C.; Hou, J. G. Probing Intramolecular Vibronic Coupling through Vibronic-State Imaging. *Nat Commun* **2021**, *12* (1), 1280. https://doi.org/10.1038/s41467-021-21571-z.
(41) Zhang, Y.; Yang, B.; Ghafoor, A.; Zhang, Y.; Zhang, Y.-F.; Wang, R.-P.; Yang, J.-L.; Luo, Y.; Dong, Z.-C.; Hou, J. G. Visually Constructing the Chemical Structure of a Single Molecule by Scanning Raman Picoscopy. *National Science Review* **2019**, *6* (6), 1169–1175. https://doi.org/10.1093/nsr/nwz180.
(42) Aguilar-Galindo, F.; Díaz-Tendero, S.; Borisov, A. G. Electronic Structure Effects in the Coupling of a Single Molecule with a Plasmonic Antenna. *J. Phys. Chem. C* **2019**, *123* (7), 4446–4456. https://doi.org/10.1021/acs.jpcc.8b11872.
(43) Candelas, B.; Zabala, N.; Koval, P.; Babaze, A.; Sánchez-Portal, D.; Aizpurua, J. Influence of Atomistic Features in Plasmon–Exciton Coupling and Charge Transfer Driven by a Single Molecule in a Metallic Nanocavity. *J. Chem. Phys.* **2024**, *161* (4), 044707. https://doi.org/10.1063/5.0216464.

(44) Frisch, M. J.; Trucks, G. W.; Schlegel, H. B.; Scuseria, G. E.; Robb, M. A.; Cheeseman, J. R.; Scalmani, G.; Barone, V.; Petersson, G. A.; Nakatsuji, H.; Li, X.; Caricato, M.; Marenich, A. V.; Bloino, J.; Janesko, B. G.; Gomperts, R.; Mennucci, B.; Hratchian, H. P.; Ortiz, J. V.; Izmaylov, A. F.; Sonnenberg, J. L.; Williams; Ding, F.; Lipparini, F.; Egidi, F.; Goings, J.; Peng, B.; Petrone, A.; Henderson, T.; Ranasinghe, D.; Zakrzewski, V. G.; Gao, J.; Rega, N.; Zheng, G.; Liang, W.; Hada, M.; Ehara, M.; Toyota, K.; Fukuda, R.; Hasegawa, J.; Ishida, M.; Nakajima, T.; Honda, Y.; Kitao, O.; Nakai, H.; Vreven, T.; Throssell, K.; Montgomery Jr., J. A.; Peralta, J. E.; Ogliaro, F.; Bearpark, M. J.; Heyd, J. J.; Brothers, E. N.; Kudin, K. N.; Staroverov, V. N.; Keith, T. A.; Kobayashi, R.; Normand, J.; Raghavachari, K.; Rendell, A. P.; Burant, J. C.; Iyengar, S. S.; Tomasi, J.; Cossi, M.; Millam, J. M.; Klene, M.; Adamo, C.; Cammi, R.; Ochterski, J. W.; Martin, R. L.; Morokuma, K.; Farkas, O.; Foresman, J. B.; Fox, D. J. Gaussian 16 Rev. B.01, 2016.

(45) Yanai, T.; Tew, D. P.; Handy, N. C. A New Hybrid Exchange–Correlation Functional Using the Coulomb-Attenuating Method (CAM-B3LYP). *Chemical Physics Letters* **2004**, *393* (1), 51–57. https://doi.org/10.1016/j.cplett.2004.06.011.

(46) Rodríguez-Ropero, F.; Casanovas, J.; Alemán, C. Ab Initio Calculations on π-Stacked Thiophene Dimer, Trimer, and Tetramer: Structure, Interaction Energy, Cooperative Effects, and Intermolecular Electronic Parameters. *Journal of Computational Chemistry* **2008**, *29* (1), 69–78. https://doi.org/10.1002/jcc.20763.

(47) Würthner, F.; Saha-Möller, C. R.; Fimmel, B.; Ogi, S.; Leowanawat, P.; Schmidt, D. Perylene Bisimide Dye Assemblies as Archetype Functional Supramolecular Materials. *Chem. Rev.* **2016**, *116* (3), 962–1052. https://doi.org/10.1021/acs.chemrev.5b00188.

(48) Starcke, J. H.; Wormit, M.; Schirmer, J.; Dreuw, A. How Much Double Excitation Character Do the Lowest Excited States of Linear Polyenes Have? *Chemical Physics* **2006**, *329* (1), 39–49. https://doi.org/10.1016/j.chemphys.2006.07.020.

(49) Christensen, R. L.; Galinato, M. G. I.; Chu, E. F.; Howard, J. N.; Broene, R. D.; Frank, H. A. Energies of Low-Lying Excited States of Linear Polyenes. *J. Phys. Chem. A* **2008**, *112* (49), 12629–12636. https://doi.org/10.1021/jp8060202.

(50) Yang, B.; Chen, G.; Ghafoor, A.; Zhang, Y.; Zhang, Y.; Zhang, Y.; Luo, Y.; Yang, J.; Sandoghdar, V.; Aizpurua, J.; Dong, Z.; Hou, J. G. Sub-Nanometre Resolution in Single-Molecule Photoluminescence Imaging. *Nat. Photonics* **2020**, *14* (11), 693–699. https://doi.org/10.1038/s41566-020-0677-y.

(51) Rosławska, A.; Kaiser, K.; Romeo, M.; Devaux, E.; Scheurer, F.; Berciaud, S.; Neuman, T.; Schull, G. Submolecular-Scale Control of Phototautomerization. *Nat. Nanotechnol.* **2024**, *19* (6), 738–743. https://doi.org/10.1038/s41565-024-01622-4.

(52) Rosławska, A.; Neuman, T.; Doppagne, B.; Borisov, A. G.; Romeo, M.; Scheurer, F.; Aizpurua, J.; Schull, G. Mapping Lamb, Stark, and Purcell Effects at a Chromophore-Picocavity Junction with Hyper-Resolved Fluorescence Microscopy. *Phys. Rev. X* **2022**, *12* (1), 011012. https://doi.org/10.1103/PhysRevX.12.011012.

(53) Johnson, P. B.; Christy, R. W. Optical Constants of the Noble Metals. *Phys. Rev. B* **1972**, *6* (12), 4370–4379. https://doi.org/10.1103/PhysRevB.6.4370.

(54) Javadi, A.; Mahmoodian, S.; Söllner, I.; Lodahl, P. Numerical Modeling of the Coupling Efficiency of Single Quantum Emitters in Photonic-Crystal Waveguides. *J. Opt. Soc. Am. B, JOSAB* **2018**, *35* (3), 514–522. https://doi.org/10.1364/JOSAB.35.000514.

(55) Dirac, P. A. M.; Bohr, N. H. D. The Quantum Theory of the Emission and Absorption of Radiation. *Proceedings of the Royal Society of London. Series A, Containing Papers of a Mathematical and Physical Character* **1997**, *114* (767), 243–265. https://doi.org/10.1098/rspa.1927.0039.

(56) Dirac, P. A. M.; Fowler, R. H. The Quantum Theory of Dispersion. *Proceedings of the Royal Society of London. Series A, Containing Papers of a Mathematical and Physical Character* **1997**, *114* (769), 710–728. https://doi.org/10.1098/rspa.1927.0071.

(57) Filter, R.; Mühlig, S.; Eichelkraut, T.; Rockstuhl, C.; Lederer, F. Controlling the Dynamics of Quantum Mechanical Systems Sustaining Dipole-Forbidden Transitions via Optical Nanoantennas. *Phys. Rev. B* **2012**, *86* (3), 035404. https://doi.org/10.1103/PhysRevB.86.035404.
(58) Rusak, E.; Straubel, J.; Gładysz, P.; Göddel, M.; Kędziorski, A.; Kühn, M.; Weigend, F.; Rockstuhl, C.; Słowik, K. Enhancement of and Interference among Higher Order Multipole Transitions in Molecules near a Plasmonic Nanoantenna. *Nat Commun* **2019**, *10* (1), 5775. https://doi.org/10.1038/s41467-019-13748-4.
(59) Spano, F. C.; Silva, C. H- and J-Aggregate Behavior in Polymeric Semiconductors. *Annual Review of Physical Chemistry* **2014**, *65* (Volume 65, 2014), 477–500. https://doi.org/10.1146/annurev-physchem-040513-103639.
(60) Neuman, T.; Esteban, R.; Casanova, D.; García-Vidal, F. J.; Aizpurua, J. Coupling of Molecular Emitters and Plasmonic Cavities beyond the Point-Dipole Approximation. *Nano Lett.* **2018**, *18* (4), 2358–2364. https://doi.org/10.1021/acs.nanolett.7b05297.
(61) Kazemi-Zanjani, N.; Vedraine, S.; Lagugné-Labarthet, F. Localized Enhancement of Electric Field in Tip-Enhanced Raman Spectroscopy Using Radially and Linearly Polarized Light. *Opt. Express, OE* **2013**, *21* (21), 25271–25276. https://doi.org/10.1364/OE.21.025271.
(62) Marquier, F.; Sauvan, C.; Greffet, J.-J. Revisiting Quantum Optics with Surface Plasmons and Plasmonic Resonators. *ACS Photonics* **2017**, *4* (9), 2091–2101. https://doi.org/10.1021/acsphotonics.7b00475.